福昕PDF编辑器

• 永久　• 轻巧　• 自由

升级会员　　批量购买

永久使用

无限制使用次数

极速轻巧

超低资源占用，告别卡顿慢

自由编辑

享受Word一样的编辑自由

扫一扫，关注公众号

Infrared Physics & Technology 76 (2016) 75–81

Contents lists available at ScienceDirect

Infrared Physics & Technology

journal homepage: www.elsevier.com/locate/infrared

Infrared small target detection via line-based reconstruction and entropy-induced suppression

Ke Shang [a], Xiao Sun [a], Jinwen Tian [a,*], Yansheng Li [b], Jiayi Ma [c]

[a] School of Automation, Huazhong University of Science & Technology, 1037 Luoyu Road, Wuhan 430074, China
[b] School of Remote Sensing and Information Engineering, Wuhan University, 299 Bayi Road, Wuhan 430072, China
[c] Electronic Information School, Wuhan University, 299 Bayi Road, Wuhan 430072, China

ARTICLE INFO

Article history:
Received 9 October 2015
Available online 4 February 2016

Keywords:
Infrared small target detection
Line-based reconstruction
Entropy-induced suppression

ABSTRACT

This paper proposes a novel infrared small target detection method which is composed of two stages. The first stage is implemented by line-based reconstruction for suppressing the background clutter, and the second stage is induced by information entropy for further standing out the targets. Compared with the state-of-the-art approaches, the proposed approach is able to achieve better performance in terms of efficiency and accuracy.

1. Introduction

Infrared small target detection has attracted lots of research interests, due to its key role in terminal guidance [1], early warning [2,3], space surveillance [4], and so forth. Due to that the target is at a far distance, its projected image is usually very small and does not have available shape and texture for detection or matching [5–8]. Furthermore, because of the effects of inherent sensor noise or environment, the obtained infrared small targets are often buried in a complex background with low signal-to-clutter ratio (SCR). Therefore, it is difficult to detect the small targets in complex infrared background.

In literature, infrared small target detection methods are mainly classified into the following categories: morphological based method [9], extreme value theory based method [10–13], statistical regression method [14], saliency based method [15] and image layering based approach [16]. Based on Top-hat filtering, some new related methods have been presented [17]. The Top-hat filtering parameters are optimized by using neural network and genetic algorithm [18]. A new Top-hat transformation method was proposed by Bai et al. [19]. They reorganized the classical Top-hat transformation by using two different but correlated structuring elements. Although large amounts of research in this field have been carried out for decades, it is still admittedly a challenging task nowadays due to the unpredictable complexity of backgrounds. Existing approaches attempt to cope with the problem from perspectives include spatial space [11], frequency domain [20], infrared spectrum [21,22], and mathematical morphology [23]; however, many of them just concern specific scenes like the sky [24] or sea-sky [25]. In general, infrared small target detection is still a difficult task because the success of these approaches is restricted to their own application domain.

In order to cope with the heavy imaging noise and kinds of complex background clutters, this paper proposes a novel approach include two stages: multi-direction line reconstruction and information entropy-induced suppression. The first stage can efficiently suppressing background clutters even under complex backgrounds (e.g., the ground background). For further standing out the targets, the second stage is proposed for refining the result of the first stage. Eventually, the aforementioned two stages jointly cope with the infrared small target detection problem. As a whole, this paper proposes a simple but effective infrared small target detection approach. Because the presented algorithm can be implemented by low computational complexity, the algorithm is fit for the on-board real-time applications.

The remainder of this paper is organized as follows. Section 2 first introduces the novel infrared small target detection approach. Section 3 gives a comprehensive analysis of the proposed aircraft target detection approach. In Section 4, a conclusion is drawn for a summary of this paper.

* Corresponding author.
E-mail addresses: shangke1988@hust.edu.cn (K. Shang), sxiao@hust.edu.cn (X. Sun), jwtian@hust.edu.cn (J. Tian), liyansheng99@gmail.com (Y. Li), jyma2010@gmail.com (J. Ma).

http://dx.doi.org/10.1016/j.infrared.2016.01.024
1350-4495/

2. The proposed infrared small target detection method

2.1. Line-based reconstruction

Generally speaking, the intensity value of the target is different from surrounding ones in all directions, while the pixels on the background structure own the consistent intensity value in at least one direction. Thus we use the most similar intensity value of surrounding pixels to reconstruct background. In infrared image, the pixel of target is typically brighter than background. In order to depict the intrinsic difference, line-based reconstruction residual is motivated for indicating the small target. Along the direction θ, the line reconstruction residual B can be calculated by

$$B(x,y,\theta) = I(x,y) - \min_{l\in(0,l_m)} I(x + l\cos\theta, y + l\sin\theta), \tag{1}$$

where I denotes the image, (x,y) is the position of a pixel, θ is the direction, l is a variable indicating the distance between a pixel and its surrounding pixel, and l_m is the upper bound of the size of targets. The residuals along $0, \pi/2, \pi$, and $3\pi/2$ are visually shown in Fig. 1*h–k*. From the residuals, we see that the background is suppressed along different directions.

The residuals means the pixel is brighter than the surrounding in direction θ. The target is brighter than the surrounding in all directions. By using the contributions from multi-directions, the small target can be indicated by the minimum response from all directions:

$$f(x,y) = \min_{\theta\in(0,2\pi]} B(x,y,\theta). \tag{2}$$

Therefore, for the pixel (x,y), it is $f(x,y)$ brighter than the minimum response to the surrounding pixels in all directions.

Benefiting from the multi-direction suppression, the small target is distinguished from the background as depicted in Fig. 1*l*. In the following stage, the small target will be further enhanced.

In order to reduce computational complexity, the calculation of Eq. (2) can be simplified by Eq. (3).

$$\begin{aligned} f(x,y) &= \min_{\theta\in(0,2\pi]}\left(I(x,y) - \min_{l\in(0,l_m)} I(x + l\cdot\cos\theta, y + l\cdot\sin\theta)\right) \\ &= I(x,y) - \max_{\theta\in(0,2\pi]}\left(\min_{l\in(0,l_m)} I(x + l\cdot\cos\theta, y + l\cdot\sin\theta)\right) \\ &= I(x,y) - \max_{\theta\in(0,2\pi]} D(x,y,\theta), \end{aligned} \tag{3}$$

where

$$D(x,y,\theta) = \min_{l\in(0,l_m)} I(x + l\cdot\cos\theta, y + l\cdot\sin\theta). \tag{4}$$

In addition, the identical Eq. (5) holds.

$$D(x,y,\theta) \equiv D(x + l_m\cdot\cos\theta, y_m + l\cdot\sin\theta, -\theta). \tag{5}$$

Hence, $D(x,y,\theta)$ can be reused in operations of different pixels which can reduce the computational complexity of our original algorithm.

In the scenes where the pixels of target are darker than background, replace Eq. (3) by Eq. (6). If it is necessary to detect bright and dark target in the same time, the maximum of Eqs. (3) and (6) could be used. And the computational complexities will be doubled.

$$f(x,y) = -I(x,y) + \min_{\theta\in(0,2\pi]}\left(\max_{l\in(0,l_m)} I(x + l\cdot\cos\theta, y + l\cdot\sin\theta)\right). \tag{6}$$

2.2. Entropy-induced suppression

In this section, information entropy [26] is utilized to refine the residual image for standing out the targets. Since large majorities of the residual image is occupied by noise, the information entropy of the target is larger than that of the noise. Hence, information

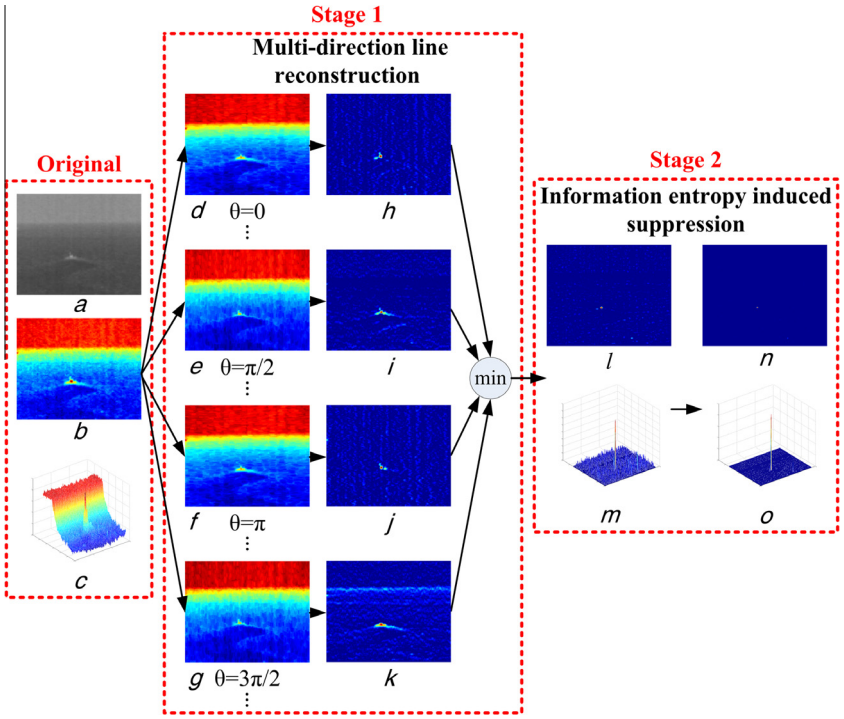

Fig. 1. The sketch of our approach. Left column: original image is shown as gray image *a*, pseudo color image *b* and distribution image *c*. Middle column: along the direction θ, the line reconstruction is shown in *d–g*; the residual is shown in *h–k*. Right column: the minimum response from all directions is shown in *l*; *m* is distribution image of *l*; the result *n* is information entropy-induced suppressed from *l*; *o* is distribution image of *n*. (For interpretation of the references to colour in this figure legend, the reader is referred to the web version of this article.)

entropy can be utilized to further distinguish targets from noise. After line-based reconstruction, the intensity value of the residual image approximately follows Gaussian distribution as verified by Fig. 2. Let f denote the intensity value of one pixel in the residual image, the probability density of f can be calculated by:

$$p(f) = \frac{1}{\sqrt{2\pi}\sigma} \exp - \frac{(f-\mu)^2}{\sigma^2}, \quad (7)$$

where μ and σ denote the mean and the standard deviation of the noise.

Based on [26], the information entropy of the intensity f can be expressed by:

$$H(f) = -\log p(f) = -\log \frac{1}{\sqrt{2\pi}\sigma} + \frac{(f-\mu)^2}{\sigma^2} = C_1 + C_2(f-\mu)^2, \quad (8)$$

where $C_1 = -\log \frac{1}{\sqrt{2\pi}\sigma}$ and $C_2 = \frac{1}{\sigma^2}$ are constants for a given specific image.

2.3. The sketch of the proposed method

Based on the aforementioned two stages, we summarize our proposed method in Algorithm 1. Generally, the whole infrared small target detection contains two steps: target enhancement and target segmentation. Algorithm 1 denotes the infrared small target enhancement process, which is the crucial step of infrared small target detection and the focus of this paper. After the target enhancement map is achieved by Algorithm 1, target segmentation can be easily implemented by statistical analysis such as constant false alarm rate (CFAR) [27], which is not specifically discussed in this paper. In addition, the enhanced maps by Algorithm 1 are specifically evaluated in the experimental section.

Algorithm 1. The proposed method

Input: Original infrared image I
Output: Target-like image H
1. Calculate the minimum response from all θ by Eq. (3);
2. Calculate the information entropy (the output) by Eq. (8).

3. Experimental results

3.1. Data set and evaluation criteria

We test our proposed method on several typical images, which are from different kinds of backgrounds, as shown in Fig. 3.

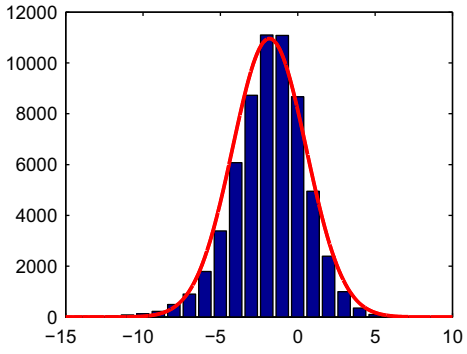

Fig. 2. The histogram of the residual image. The blue bars represent the histogram of the residual image shown in Fig. 1*l*, and the red line denotes its corresponding Gaussian distribution fitting curve. (For interpretation of the references to colour in this figure legend, the reader is referred to the web version of this article.)

Information of targets is shown in Table 1, where we also provide the local signal-to-clutter ratio (SCR) on the target areas (30×30 windows). The SCR is defined as

$$SCR = \frac{|f_T - \mu|}{\sigma}, \quad (9)$$

where f_T is point target intensity value, μ is background mean intensity, and σ is background standard deviation.

In our experiments, we use SCR Gain [28], background suppression factor (BSF) [28], and receiver operation characteristic (ROC) curves [14] to evaluate the performance. SCR Gain is by far the most common metric used in the evaluation of infrared small target detection. It is a measure of the improvement in the SCR after proceeding. The BSF ignores the signal and looks only at the clutter suppression. The SCR Gain and BSF are defined as follows:

$$SCR\ \ Gain = \frac{SCR_{out}}{SCR_{in}}, \qquad BSF = \frac{\sigma_{in}}{\sigma_{out}}. \quad (10)$$

The ROC curve represents the varying relationship of the detection probability P_d and false alarm rate P_f. The P_d is calculated as the number ratio of correctly detected targets to totally real targets, and the P_d is calculated as the number ratio of incorrectly detected targets to totally detected targets.

Our algorithm involves two constants to be set, i.e., C_1 and C_2 in Eq. (8). However, their values do not influence the experimental results. The detail reasons are given as follows.

In Eq. (8), by defining $G = (f-\mu)^2$, we have $H = C_1 + C_2 * G$ and then the SCR_{out} becomes

$$SCR_{out} = SCR_H = \frac{|H - \mu_H|}{\sigma_H} = \frac{|(C_1 + C_2 * G) - (C_1 + C_2 * \mu_G)|}{C_2 * \sigma_G} = \frac{|G - \mu_G|}{\sigma_G} = SCR_G, \quad (11)$$

which means that the SCR gain value of H is independent of C_1 and C_2.

The BSF is a variation on the SCR gain, it is not meant to give a full measure of a filter's performance for clutter removal [28]. Instead, it is meant to aid in the understanding of a filter's performance. A method which has a high BSF but a low SCR gain will suspend both signal and clutter. So a method with high BSF is not always better than a low one.

Finally, for a given result image, its ROC curve will not change if we make a linear transformation on its intensity. More specifically, by defining $T_G = (T_H - C_1)/C_2$, the threshold T_H on H and the threshold T_G on G will have the same result, e.g., the same detection probability P_d and false alarm rate P_f. Therefore, the values of C_1 and C_2 do not influence the results either, and hence we simply set $C_1 = 0$ and $C_2 = 1$ throughout our experiments.

3.2. Evaluation of performance

Fig. 3 presented the qualitative comparisons on the test images with other five state-of-the-art methods such as Top-Hat [9], LS-SVM [10], Facet [11], MFM [12], and DSVT[13]. Fig. 3*a–c* denote the sea-sky background case, Fig. 3*d–g* illustrate the ground background scenario, and Fig. 3*h–j* demonstrate the sky background scene. The results of line-based reconstruction in our method are shown in the second last column in Fig. 3, where we set $\theta \in \{\frac{n}{6}\pi | n = 1, 2, \ldots, 12\}$ and $l_m = 6$ throughout the experiments. In order to further reduce the computational complexity, we take l in discrete values $l \in \{2, 4, 6\}$. The final results of our method are given in the last column in Fig. 3. Obviously, our method has the best performance, and the result images are much cleaner than those of the other methods.

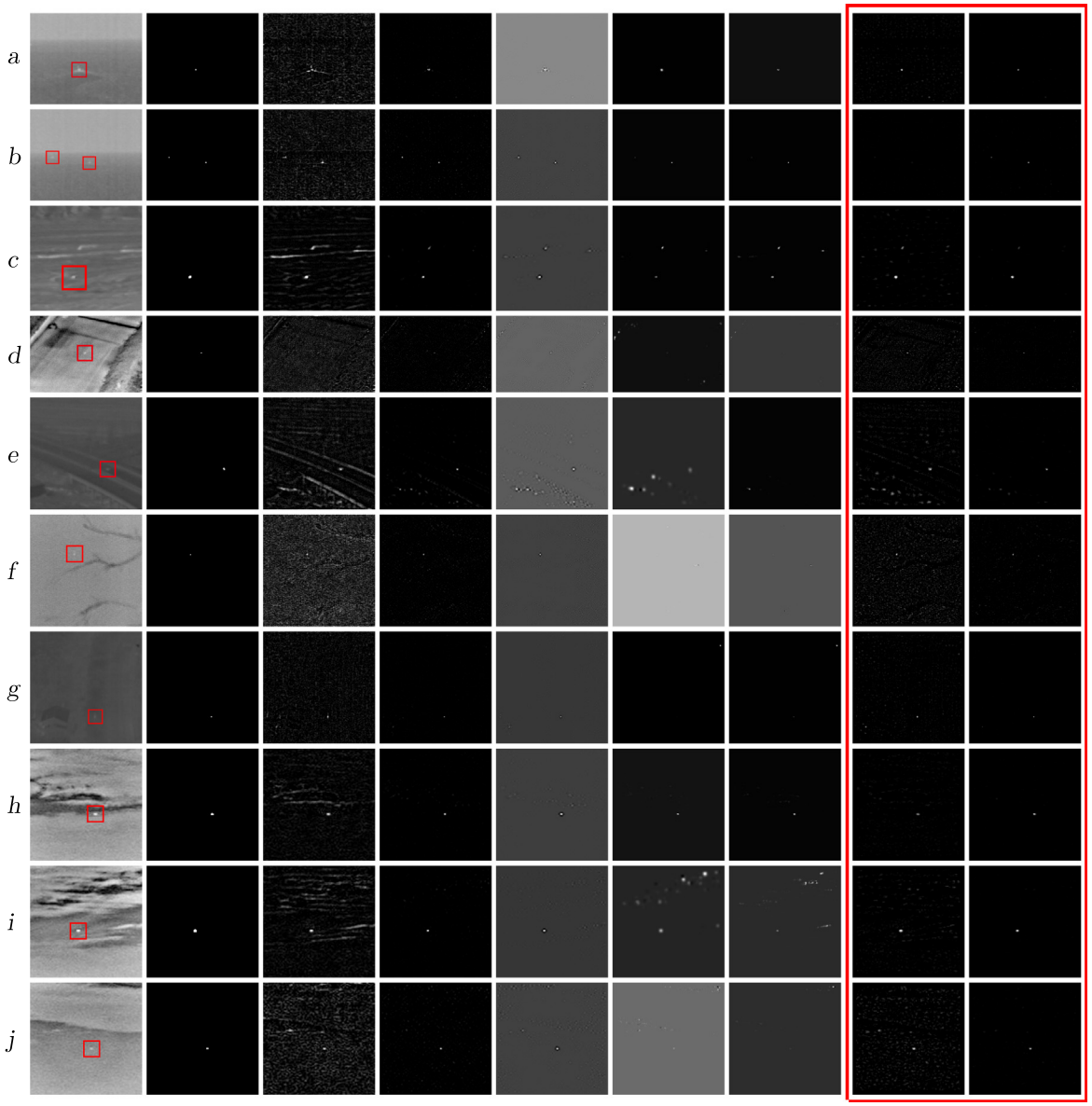

Fig. 3. Small infrared target detection results on several typical images of our proposed method compared with other five methods. For each row, maps from left to right are: Original image, Ground-truth, Top-Hat [9], LS-SVM [10], Facet [11], MFM [12], DSVT [13], Our approach (1st stage), Our approach (1st stage + 2nd stage).

Table 1
Information of infrared small targets.

Images	Scene	Size	SCR[a]
a	Sea	5×5	3.87
b	Sea	4×4, 4×3	1.77, 3.11
c	Sea	4×4	7.53
d	Ground	4×4	4.57
e	Ground	2×2	3.26
f	Ground	3×3	6.65
g	Ground	2×4	5.98
h	Sky	4×3	3.38
i	Sky	3×2	5.53
j	Sky	2×2	6.15

[a] SCR use a 30×30 window.

We next report the quantitative results for each image in Fig. 3. The ROC curves of the detection results are shown in Fig. 4. We see that the ROC curves of our approach are consistently above those of the other five methods, which intuitively show that our approach can achieve better performance than existing approaches.

The SCR Gain and BSF are listed in Table 2. From the results, we see that our method achieves the best SCR Gain and BSF on most of the ten scenes. We also provide the results of our method using just the 1st stage in the table, which demonstrate that the information entropy use in the second stage does play an important role for target enhancement.

The top-hat transformation has been used for small target detection since many years, but the ability of target detection is weak. The LS-SVM model and Facet model are based on extreme value theory. They achieve better performance than The top-hat transformation. The MSF model and DSVT model use multiscale information of images. They can work very well in a flat background. But in a complex background, there are many false alarms in their results. In generally, our approach can achieve better performance than existing approaches in most of images.

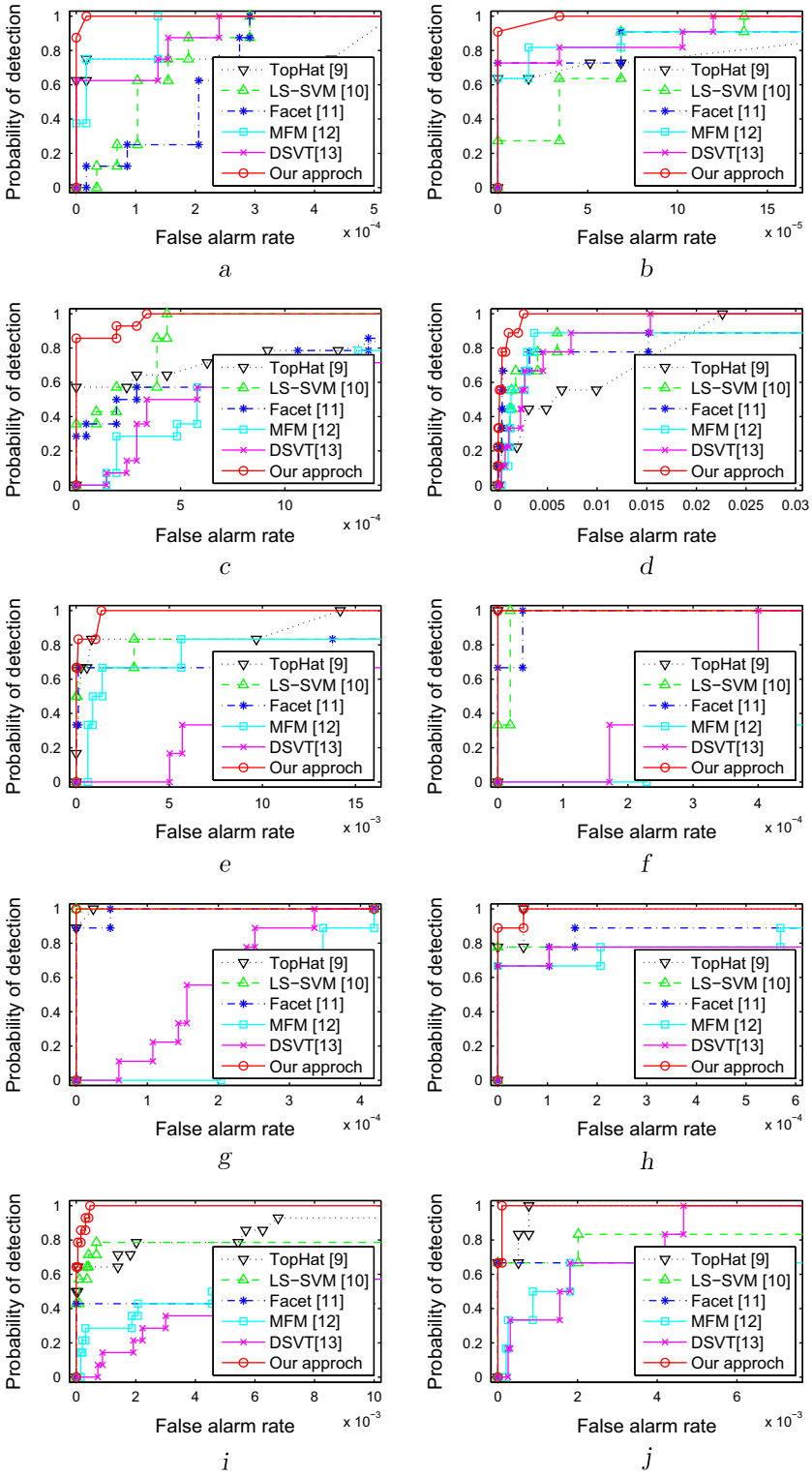

Fig. 4. ROC curves of the six methods on the ten images in Fig. 3.

3.3. Computational complexities

We analyze the computational complexities of our method. In our method, there are 12 minimum operations, 11 maximum operations, 3 subtraction operations and 1 square operation per pixel. The computational complexities of different methods are listed in Table 3. From Table 3, we see that the computational complexities of our method are less than that of others.

We compare the run times of the involved six methods in Fig. 5, which is listed in Table 2. The experiments are implemented on a

Table 2
Quantitative comparisons on the ten images in Fig. 3.

Methods	Indicators	Image *a*	Image *b*	Image *c*	Image *d*	Image *e*
Part I						
Top-Hat [9]	SCR Gain	6.18	17.32	1.96	1.80	4.41
	BSF	1.51	1.59	0.56	1.84	0.27
	Time (ms)	16.72	10.68	7.15	12.08	9.97
LS-SVM [10]	SCR Gain	25.85	69.70	7.91	5.73	18.55
	BSF	9.62	7.29	4.36	5.06	1.29
	Time (ms)	8.25	7.47	4.06	8.29	3.56
Facet [11]	SCR Gain	14.77	75.17	4.25	4.37	9.33
	BSF	11.90	10.54	3.76	6.33	0.95
	Time (ms)	10.95	11.03	5.47	15.74	5.65
MFM [12]	SCR Gain	73.16	533.97	2.46	2.52	4.56
	BSF	22.26	86.38	3.09	19.74	1.92
	Time (ms)	40.89	44.74	25.57	52.52	26.46
DSVT [13]	SCR Gain	79.98	**584.51**	3.11	2.03	0.06
	BSF	28.69	**105.05**	2.40	**22.42**	2.21
	Time (ms)	45.32	48.29	25.47	59.80	23.57
Our approach (1st stage)	SCR Gain	22.34	41.83	6.91	5.84	12.87
	BSF	**55.96**	52.60	**10.32**	13.40	**9.71**
Our approach (1st stage + 2nd stage)	SCR Gain	**120.40**	188.25	**20.63**	**15.14**	**38.58**
	BSF	35.00	24.51	8.51	10.97	3.19
	Time (ms)	**7.38**	**6.14**	**3.47**	**7.86**	**3.19**
		Image *f*	Image *g*	Image *h*	Image *i*	Image *j*
Part II						
Top-Hat [9]	SCR Gain	1.49	3.51	4.20	4.15	3.36
	BSF	0.34	0.35	2.41	2.28	0.91
	Time (ms)	10.71	14.19	7.84	10.38	7.17
LS-SVM [10]	SCR Gain	8.47	21.74	22.02	29.46	17.88
	BSF	2.16	3.05	19.44	27.24	5.56
	Time (ms)	6.41	8.50	3.36	4.01	3.88
Facet [11]	SCR Gain	8.43	16.93	12.41	10.24	13.31
	BSF	2.90	3.23	13.99	18.10	6.00
	Time (ms)	12.04	16.37	5.38	5.94	5.38
MFM [12]	SCR Gain	1.56	0.78	47.58	4.40	3.95
	BSF	9.35	2.23	**58.41**	10.31	7.49
	Time (ms)	35.11	48.32	19.93	18.19	20.83
DSVT [13]	SCR Gain	1.95	5.26	35.31	2.08	1.86
	BSF	**9.69**	1.98	38.62	6.91	8.77
	Time (ms)	40.72	63.97	21.60	23.68	21.54
Our approach (1st stage)	SCR Gain	2.94	8.05	10.82	17.31	8.56
	BSF	4.44	**13.66**	14.02	16.83	9.47
Our approach (1st stage + 2nd stage)	SCR Gain	**9.55**	**69.42**	**62.60**	**85.69**	**38.37**
	BSF	2.18	11.09	52.95	**67.79**	**12.97**
	Time (ms)	**6.10**	**7.81**	**2.94**	**3.00**	**3.26**

The bold values are the best value of each image.

laptop with 2.5 GHz Intel Core i5 CPU, 4 GB memory and Matlab code. Obviously, our method can achieve the best efficiency under different situations. Hence, our method fits for the real-time applications. As a whole, the proposed method can achieve better performance than existing approaches in terms of accuracy and efficiency.

Table 3
The arithmetic operation number of different methods.

Methods	The arithmetic operation number per pixel			
	+,−	min,max	*	^2
Top-Hat [9]	1	50	0	0
LS-SVM [10]	0	0	51	0
Facet [11]	1	0	77	1
MFM [12]	0	0	311	0
DSVT [13]	0	0	375	0
Our approach	3	23	0	1

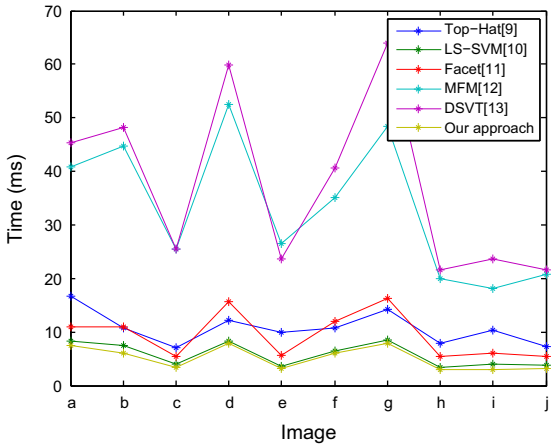

Fig. 5. The time spent by the six methods on the ten images in Fig. 3.

4. Conclusion

In this paper, we introduce a small target detection method in infrared images based on line-based reconstruction and entropy-induced suppression. The proposed algorithm can work well under different kinds of backgrounds. Qualitative and Quantitative evaluation results demonstrate that the proposed method can achieve better accuracy and efficiency performance compared with state-of-the-art methods.

Conflict of interest

The authors declare no conflict of interest.

Acknowledgements

This research was supported by the National Natural Science Foundation of China (NSFC) project under Grant Nos. 61503288, 61273279 and 61371339, and by the China Postdoctoral Science Foundation under Grant No. 2015M570665. And we are also grateful to the reviewers for their suggestions.

References

[1] S. Qi, J. Ma, H. Li, S. Zhang, J. Tian, Infrared small target enhancement via phase spectrum of quaternion fourier transform, Infrared Phys. Technol. 62 (2014) 50–58.
[2] Z. Chen, T. Deng, L. Gao, H. Zhou, S. Luo, A novel spatial–temporal detection method of dim infrared moving small target, Infrared Phys. Technol. 66 (2014) 84–96.
[3] X. Yang, Y. Zhou, D. Zhou, R. Yang, Y. Hu, A new infrared small and dim target detection algorithm based on multi-directional composite window, Infrared Phys. Technol. 71 (2015) 402–407.
[4] Z.-Z. Li, J. Chen, Q. Hou, H.-X. Fu, Z. Dai, G. Jin, R.-Z. Li, C.-J. Liu, Sparse representation for infrared dim target detection via a discriminative over-complete dictionary learned online, Sensors 14 (6) (2014) 9451–9470.

[5] J. Ma, J. Zhao, J. Tian, A.L. Yuille, Z. Tu, Robust point matching via vector field consensus, IEEE Trans. Image Process. 23 (4) (2014) 1706–1721.
[6] J. Ma, W. Qiu, J. Zhao, Y. Ma, A.L. Yuille, Z. Tu, Robust L_2E estimation of transformation for non-rigid registration, IEEE Trans. Signal Process. 63 (5) (2015) 1115–1129.
[7] J. Ma, J. Zhao, A.L. Yuille, Non-rigid point set registration by preserving global and local structures, IEEE Trans. Image Process. 25 (1) (2016) 53–64.
[8] J. Ma, H. Zhou, J. Zhao, Y. Gao, J. Jiang, J. Tian, Robust feature matching for remote sensing image registration via locally linear transforming, IEEE Trans. Geosci. Remote Sensing 53 (12) (2015) 6469–6481.
[9] V.T. Tom, T. Peli, M. Leung, J.E. Bondaryk, Morphology-based algorithm for point target detection in infrared backgrounds, Proc. SPIE 1954 (1993) 2–11, http://dx.doi.org/10.1117/12.157758. http://dx.doi.org/10.1117/12.157758.
[10] P. Wang, J. Tian, C.Q. Gao, Infrared small target detection using directional highpass filters based on ls-svm, Electron. Lett. 45 (3) (2009) 156–158.
[11] G.-D. Wang, C.-Y. Chen, X.-B. Shen, Facet-based infrared small target detection method, Electron. Lett. 41 (22) (2005) 1244–1246.
[12] C. Yang, J. Ma, M. Zhang, S. Zheng, X. Tian, Multiscale facet model for infrared small target detection, Infrared Phys. Technol. 67 (2014) 202–209.
[13] C. Yang, J. Ma, S. Qi, J. Tian, S. Zheng, X. Tian, Directional support value of gaussian transformation for infrared small target detection, Appl. Opt. 54 (9) (2015) 2255–2265.
[14] Y. Gu, C. Wang, B. Liu, Y. Zhang, A kernel-based nonparametric regression method for clutter removal in infrared small-target detection applications, IEEE Geosci. Remote Sensing Lett. 7 (3) (2010) 469–473.
[15] S. Qi, D. Ming, J. Ma, X. Sun, J. Tian, A robust method for infrared small target detection based on boolean map visual theory, Appl. Opt. 53 (18) (2014) 3929–3940.
[16] H. Li, Y. Tan, Y. Li, J. Tian, Image layering based small infrared target detection method, Electron. Lett. 50 (1) (2014) 42–44.
[17] J.-l. GU, W. Zhang, M. Wan, Faint targets detection based on gray morphological filtering and neighborhood entropy method, High Power Laser Particle Beams 12 (2004) 008.
[18] M. Zeng, J. Li, Z. Peng, The design of top-hat morphological filter and application to infrared target detection, Infrared Phys. Technol. 48 (1) (2006) 67–76.
[19] X. Bai, F. Zhou, Analysis of new top-hat transformation and the application for infrared dim small target detection, Pattern Recogn. 43 (6) (2010) 2145–2156.
[20] S. Qi, J. Ma, H. Li, S. Zhang, J. Tian, Infrared small target enhancement via phase spectrum of quaternion fourier transform, Infrared Phys. Technol. 62 (2014) 50–58.
[21] H. Liu, L. Yan, Y. Chang, H. Fang, T. Zhang, Spectral deconvolution and feature extraction with robust adaptive tikhonov regularization, IEEE Trans. Instrument. Measure. 62 (2) (2013) 315–327.
[22] H. Liu, Z. Zhang, S. Liu, T. Liu, L. Yan, T. Zhang, Richardson–lucy blind deconvolution of spectroscopic data with wavelet regularization, Appl. Opt. 54 (7) (2015) 1770–1775.
[23] W. Meng, T. Jin, X. Zhao, Adaptive method of dim small object detection with heavy clutter, Appl. Opt. 52 (10) (2013) D64–D74.
[24] E. Vasquez, F. Galland, G. Delyon, P. Réfrégier, Mixed segmentation-detection-based technique for point target detection in nonhomogeneous sky, Appl. Opt. 49 (9) (2010) 1518–1527.
[25] L. Yang, J. Yang, K. Yang, Adaptive detection for infrared small target under sea-sky complex background, Electron. Lett. 40 (17) (2004) 1083–1085.
[26] C.E. Shannon, A mathematical theory of communication, ACM SIGMOBILE Mobile Comput. Commun. Rev. 5 (1) (2001) 3–55.
[27] S. Kim, J. Lee, Small infrared target detection by region-adaptive clutter rejection for sea-based infrared search and track, Sensors 14 (7) (2014) 13210–13242.
[28] C.I. Hilliard, Selection of a clutter rejection algorithm for real-time target detection from an airborne platform, in: AeroSense 2000, International Society for Optics and Photonics, 2000, pp. 74–84.